IEEE Access
Multidisciplinary | Rapid Review | Open Access Journal

Received 16 June 2023, accepted 2 July 2023, date of publication 6 July 2023, date of current version 13 July 2023.

Digital Object Identifier 10.1109/ACCESS.2023.3292933

RESEARCH ARTICLE

Sensorless Variable Admittance Control for Human–Robot Interaction of a Dual-Arm Social Robot

JAEUK CHO[1], DONGWOON CHOI[1,2], AND JONG HYEON PARK[1], (Member, IEEE)
[1]School of Mechanical Engineering, Hanyang University, Seoul 04763, South Korea
[2]Korea Institute of Industrial Technology (KITECH), Ansan 426-171, South Korea

Corresponding author: Jong Hyeon Park (jongpark@hanyang.ac.kr)

This work was supported by the Korea Institute of Industrial Technology through the "Development of soft robotics technology for human–robot coexistence care robots" under Grant KITECH EH230015.

ABSTRACT These days, physical human-robot interaction (pHRI) of social robots has received a lot of attention. This paper proposes a method for variable admittance control (VAC) based pHRI to enable social robots to perform various social gestures. The proposed method includes several schemes. Firstly, a scheme to adjust the robot's damping is proposed, which takes into account the external torques exerted by the user and the robot's pose to control movement speed, reflecting the workspaces of both the human and the robot. Secondly, a scheme to change the joint stiffness is proposed, considering the reference angle and the external forces from the user to generate active motions for cooperative pHRI. Additionally, a scheme to change the robot reference point is proposed, which adjusts based on the user's external forces and the robot's posture for pHRI in various situations. The proposed methods are implemented with a dual-arm social robot. To realize pHRI based on the proposed schemes, a generalized momentum-based disturbance observer, one of the sensorless disturbance observers, is employed to estimate the exerted torque. To verify the performance of the proposed methods, experiments are carried out for handshaking and hugging.

INDEX TERMS Physical human–robot interaction, social robots, variable admittance control.

I. INTRODUCTION

These days, there is a growing interest in physical human-robot interaction (pHRI) to support people, and it has been applied in various fields, including industries, services, education, and healthcare [1], [2], [3], [4]. Specially, pHRI plays an important role in the field of social robots, which are designed to support people in an interpersonal manner to achieve social or emotional goals [5], through physical contacts that are important in social interaction [3], [4]. For this reason, many studies to realize the pHRI of social robots have been carried out [6], [7], [8], [9], [10]. Some of these studies have proposed methods based on predefined trajectories and models, such as central pattern generators (CPG), to generate social interaction motions, such as hugging or handshaking of robots [11], [12], [13]. However, these kinds of methods are specialized for one kind of motion pattern, making it challenging to adapt to various situations. To overcome this problem and realize pHRI, studies for pHRI based on the user's external force have been carried out. Admittance control, which is a position-based impedance control, has been employed as one of the force-based approaches for pHRI. [14], [6].

The admittance control scheme has been commonly applied to realize pHRI because it can be adapted to position-control based robots and is robust to uncertainty in the robot dynamics [15]. To realize pHRI in various situations, motion generation according to human intentions and tasks is necessary, and various methods based on variable admittance control (VAC), which change admittance parameters according to the environment, have been proposed. One of the proposed schemes is the analytic

The associate editor coordinating the review of this manuscript and approving it for publication was Tao Liu.

model-based method. Yusuke proposed a minimum jerk model to estimate human motion [16], and analytical models based on the estimated stiffness of the human arm were also proposed [17], [18], [19]. Using the analytical model-based schemes, the admittance parameters could be adjusted according to the user's motion. However, the drawback of these methods is the requirement of a predefined analytic model, which is heavily influenced by the uncertainties of the simplified models [20]. To address the problem of model uncertainties, methods based on learning were proposed [21], [22], [23]. However, these methods require a significant amount of training data, which can be inconvenient to collect and implement for various behaviors [24].

To address the problems and generate various motions for social interaction, such as handshaking and hugging, this paper proposes a motion generation method based on variable admittance control (VAC). In social interaction between humans and robots, it is necessary to generate motion according to the operator's intention [14] and consider the range of motion of human joints to create human-like motion [4]. Additionally, active motion of the social robot is needed for the social interaction of both participants, i.e. human and the robot [25]. In order to meet the needs for pHRI of social robots and realize the motion, this paper proposes a method based on variable admittance parameters designed through the following schemes. Firstly, a scheme to change damping at the robot based on the user's external torques and the motion of the robot is proposed to adjust the robot's movement speed according to the user's intention while reflecting the movable range of a human and robot, simultaneously. Secondly, a variable joint stiffness is proposed to generate active motions for cooperative pHRI based on the reference point and the external torques exerted by the user. Additionally, a scheme is proposed to change the reference point based on the external torques to generate interaction motion for different situations.

Generally, admittance control-based methods require force sensors to measure external forces. However, using sensors for pHRI has several drawbacks, such as increased joint design complexity, limited performance, and higher manufacturing costs [26]. To address this issue, several studies have proposed solutions, including the use of a generalized momentum (GM)-based disturbance observer [27], [28]. In this paper, a GM-based disturbance observer is employed to estimate human external torque without additional torque sensors, and the estimated torque is used to generate motions for pHRI. The proposed method is validated by performing social gestures, such as handshaking and hugging, in various situations. The key contributions made by this paper are:

1) A VAC-based method is proposed to generate pHRI motions for the various social gestures.
2) It was demonstrated that the VAC-based method was realized to the social robot called EveR6 without additional torque sensors based on a GM-based disturbance observer.

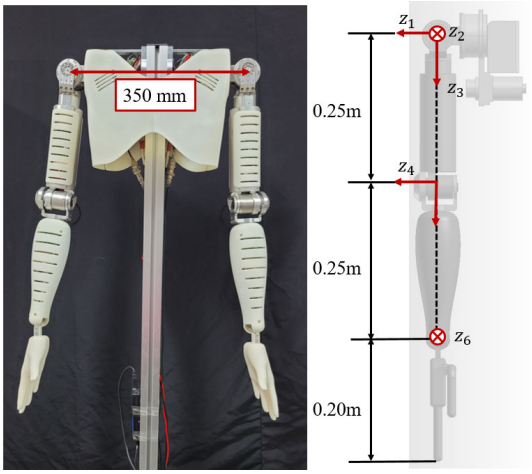

FIGURE 1. EVer6.

3) The proposed methods were validated through experiments where social gestures such as handshaking and hugging were successfully performed in various situations.

The remainder of this paper is organized as follows. Section II introduces the dual-arm social robot called EveR6, and Section III explains how to apply the sensorless disturbance observer based on GM. Section IV explains the proposed method for VAC-based motion generation. In Section V, the performance of the proposed method is measured, and its effectiveness is demonstrated through experiments. Finally, Section VI presents the conclusions.

II. MODEL DESCRIPTION

In this paper, the proposed method is realized using a dual-arm social robot named EveR6, which was developed by the Korea Institute of Industrial Technology (KITECH). EveR6 was designed based on a female body size, with a body width of 350 mm and a total arm length of 0.7 m as shown in Fig. 1. The robot has two arms with a symmetrical structure, and each arm has 6 degree-of-freedom (DOF), where z_i denotes the rotation direction of the ith joint.

The proposed methods are implemented using selected joints that are primarily utilized by the robot to perform social gestures. Assuming that n joints are used to realize the social gestures, the dynamic model of the robot can be described as follows:

$$\tau = M(q)\ddot{q} + C(q,\dot{q})\dot{q} + G(q) + \tau_f + \tau_{ext}, \tag{1}$$

where $q \in \mathbb{R}^n$ is the joint angle and $M(q) \in \mathbb{R}^{n\times n}$ is the inertia matrix, $C(q,\dot{q}) \in \mathbb{R}^{n\times n}$ is the joint torque due to Coriolis and centrifugal effects, $G(q) \in \mathbb{R}^n$ and $\tau_{ext} \in \mathbb{R}^n$ denote the joint torque due to gravity and external torque, respectively. $\tau_f \in \mathbb{R}^n$ denotes joint torque by friction, which is expressed based on the Coulomb and viscous friction model, which is used for parameter identification problems [30], [31]:

$$\tau_f = \mu_v\dot{q} + \mu_c \text{sign}(\dot{q}), \tag{2}$$

where μ_v is the viscous friction coefficient and μ_c is the coulomb friction coefficient. By substituting eq. (2) to eq. (1), the dynamic model is expressed as

$$\tau = M(q)\ddot{q} + C(q,\dot{q})\dot{q} + G(q) + \tau_{ext} + \mu_v\dot{q} + \mu_c \text{sign}(\dot{q}). \tag{3}$$

The implemented disturbance observer uses the dynamic model to estimate external forces without requiring additional sensors. The details of this observer are explained in the next section.

III. SENSORLESS DISTURBANCE OBSERVER BASED ON GENERALIZED MOMENTUM

A. PARAMETER IDENTIFICATION

In order to estimate the external torque exerted by the user based on the dynamic model without additional torque sensor, information about the dynamic parameters of the robot, such as its weight, length, and position of the mass center of each link, is needed. For identification of the dynamic parameters, in this paper, the dynamic model is expressed as a parameter estimation problem using linear observation models [31], [32], [33]. The dynamic model of the robot, eq. (3), is rewritten in the form of a linear regression as:

$$\tau = Y(q,\dot{q},\ddot{q})\phi_s, \tag{4}$$

where $Y(q,\dot{q},\ddot{q})$ is the regression matrix of a nonlinear function of joint position, velocity, and acceleration vectors. ϕ_s denotes the inertial parameters of the dynamic model, and it can be estimated through identification procedures. Firstly, the data of τ, q, and $\dot{q}$ are measured at multiple points along an excitation trajectory. When a sufficient amount of data according to the excitation trajectory is available in the time interval, $t = kT \quad (k = 1, 2, \ldots, N)$, the dimensional regression equation is constructed as follows

$$\hat{\tau} = \hat{Y}(q,\dot{q},\ddot{q})\phi_s, \tag{5}$$

where

$$\hat{\tau} = [\tau(T), \tau(2T), \cdots, \tau(NT)]^T,$$
$$\hat{Y}(q,\dot{q},\ddot{q}) = [Y(T), Y(2T), \cdots, Y(NT)]^T,$$

T denotes the step-time interval. The motor torque, i.e. τ, can be obtained by measuring the current feedback of the motor driver and using the torque coefficient of the motors:

$$\tau = N_m K_m I_m, \tag{6}$$

where N_m, I_m, and K_m denote the gear ratio of each joint, feedback current, and torque coefficient of the motors, respectively.

From the measured data, the estimation problem is formulated. Typically, the problem is solved using the least squares method. However, the obtained solution has many possibilities that satisfy the minimum norm solution, and this may not satisfy physical feasibility, such as the requirement for positive mass and inertia [33]. In this paper, to solve the problem and estimate the parameters while maintaining their physical feasibility, a parameter identification method based on a constrained quadratic problem is employed, as follows:

$$\min_{\phi_s} ||\hat{\tau} - \hat{Y}(q,\dot{q},\ddot{q})\phi_s||^2, \tag{7}$$

subject to

$$\underline{\phi}_s < \phi_s < \overline{\phi}_s,$$

where $\underline{\phi}_s$ and $\overline{\phi}_s$ respectively denote the upper and lower boundaries of the dynamic parameters, which are calculated based on the CAD data of the robot and measured mass of each link of the robot.

For effective estimation of the robot's dynamic parameters, an appropriate excitation trajectory is required. In this paper, the excitation trajectories, which are finite sum of harmonic sine and cosine functions [31], are applied as follows:

$$q_i(t) = \sum_{l=1}^{N} \frac{a_l}{\omega_f l}\sin(\omega_f l t) - \frac{b_l}{\omega_f l}\cos(\omega_f l t) + q_{i0}, \tag{8}$$

$$\dot{q}_i(t) = \sum_{l=1}^{N} a_l \cos(\omega_f l t) + b_l \sin(\omega_f l t), \tag{9}$$

$$\ddot{q}_i(t) = \sum_{l=1}^{N} \omega_f l(b_l \cos(\omega_f l t) - a_l \sin(\omega_f l t)), \tag{10}$$

where q_i, $\dot{q}_i$, and $\ddot{q}_i$ respectively denote the angle, angular velocity, and angular acceleration for the ith joint of the robot; ω_f and q_{i0} denote the fundamental frequency and the offset angle of the ith joint, respectively. The amplitudes of the cosine and sine functions are determined by the parameters a_l and b_l, which were selected by considering the actuation range of the ith joint. In this paper, the excitation trajectories are generated for the first, second, and fourth joints, which are mainly used for the robot to perform social gestures, such as handshaking and hugging. The parameters are determined by considering the robot's workspace and driving range during the social gestures, where the amplitude of the trajectories is designed to be equal because the driving range of the joints is the same. The parameters for the excitation trajectories are summarized in Tables 1 and 2.

TABLE 1. Motion range and frequency for the identification.

i	Motion range	q_{i0}	ω_f	Driving range
1	$-30 \sim 80$ degrees	10 degrees	1.57 rad/s	110 degrees
2	$0 \sim 110$ degrees	40 degrees	1.57 rad/s	110 degrees
4	$0 \sim 110$ degrees	40 degrees	1.57 rad/s	110 degrees

TABLE 2. The parameters for the excitation trajectories. ($N = 5$).

l	1	2	3	4	5
a_l	15	-10	15	15	-10
b_l	15	-10	15	15	-10

The data for identification is collected with the excitation trajectories, assuming that there are no external torques, i.e. $\tau_{ext} = 0$, and parameter identification is carried out based

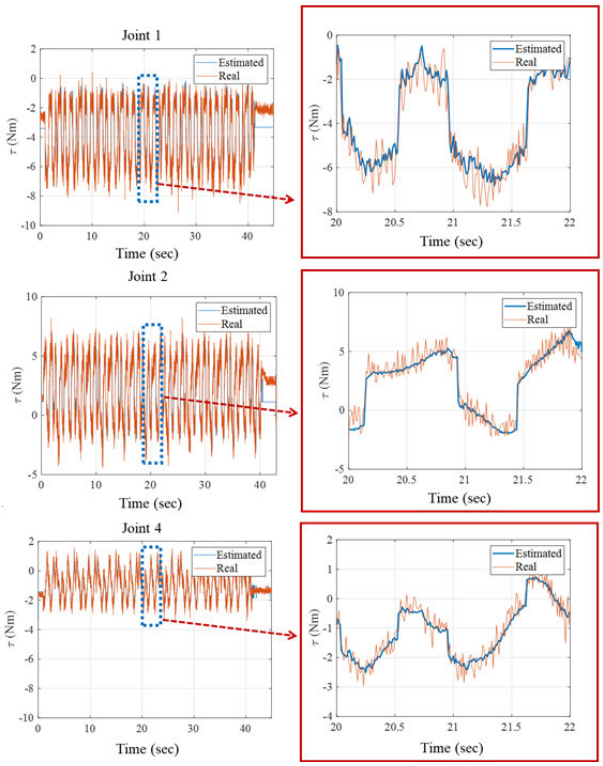

FIGURE 2. Comparison between measured and estimated torque of joints.

on the collected data. Fig. 2 shows motor torques that are calculated with the measured data, i.e. I_m, and estimated torques that are calculated based on eq. (1) with the identified parameters. The estimated torques are similar to the measured torques, and the total root mean square error between the measured and estimated torques is 0.697, as shown in Fig. 2. These results confirm that the robot's dynamic parameters have been successfully identified.

By applying the estimated dynamic parameters to eq. (3), the external torque, i.e. τ_{ext}, can be computed. However, the angular acceleration, i.e. $\ddot{q}$, which is obtained by differentiating the measured joint angle, i.e. q, and joint velocity, i.e. $\dot{q}$, can include amplified measurement noise, and this can negatively impact the performance of the disturbance observer. In order to mitigate this problem, in this paper, a GM-based disturbance observer is applied.

B. DISTURBANCE OBSERVER BASED ON GENERALIZED MOMENTUM

The GM based disturbance observer was proposed to avoid the problems of traditional methods such as noise caused by the computation of joint accelerations or the inversion of the inertia matrix [29]. The GM of the robot can be expressed as:

$$p = M(q)\dot{q} \in \mathbb{R}^n, \tag{11}$$

and thus

$$\dot{p} = M(q)\ddot{q} + \dot{M}(q)\dot{q}. \tag{12}$$

By substituting (12) into (1), the equation can be expressed as

$$\dot{p} = \dot{M}(q)\dot{q} - C(q,\dot{q})\dot{q} - G(q) - \tau_f + \tau - \tau_{ext}. \tag{13}$$

With skew-symmetry property of $M(q)$, i.e. $\dot{M}(q) = C(q,\dot{q}) + C^T(q,\dot{q})$, the equation can be expressed as follows:

$$\dot{p} = \bar{\tau} - \tau_f - \tau_{ext}, \tag{14}$$

where

$$\bar{\tau} = C^T(q,\dot{q})\dot{q} - G(q) + \tau.$$

From eq. (14), the dynamic model can be expressed without joint acceleration and inversion of the inertia matrix. The observer according to the GM is defined:

$$\dot{\hat{p}} = \bar{\tau} - \tau_f - L(p - \hat{p}), \tag{15}$$

where p can be calculated based on the estimated dynamic parameters and measured q and $\dot{q}$. Then, the external force, i.e. $\hat{\tau}_{ext}$, can be expressed:

$$\hat{\tau}_{ext} = L(p - \hat{p}), \tag{16}$$

where $L \in \mathbb{R}^{n\times n}$ is the positive gain of observer. By using the disturbance observer based on GM, external torque of each joint is estimated with feedback current and angle from the motor driver and encoder without additional torque sensors. In this paper, the estimated torque is utilized to generate motion for pHRI by applying it to VAC. The proposed schemes of VAC are presented in the next section.

IV. VARIABLE ADMITTANCE CONTROL FOR HUMAN ROBOT INTERACTION

Admittance control is a control method that produces compliant motion in response to external forces. The dynamic behavior of admittance control is governed by the admittance parameters, namely mass, damping, and stiffness. Therefore, selecting the appropriate admittance parameters based on the user's intent is crucial for pHRI. In this paper, a VAC-based method is proposed for generating motion in social interactions with humans. When applying admittance control to m joints, the VAC model is designed in the joint space as follows.

$$M\ddot{\tilde{\theta}} + B_v\dot{\tilde{\theta}} + K_v\tilde{\theta} = \tilde{\tau}_{ext}, \tag{17}$$

where

$$\tilde{\theta} = \theta_d - \theta_m,$$
$$\tilde{\tau}_{ext} = \tau_d - \tau_{ext},$$

$\theta_d \in \mathbb{R}^m$ and $\theta_m \in \mathbb{R}^m$ denote reference and modified trajectories, respectively; M, B_v, and K_v denote $m \times m$ symmetrical positive definite matrices, which mean admittance parameters, i.e. mass, damper, and stiffness, respectively; $\tau_d \in \mathbb{R}^m$ and $\tau_{ext} \in \mathbb{R}^m$ denote desired and actual external torques, respectively. In this paper, the variable damping and stiffness, i.e. B_v and K_v, are applied to reflect the user's intention. From

eq. (17), the modified acceleration with respect to the external torques are obtained as follows.

$$\ddot{\theta}_m = \ddot{\theta}_d + M^{-1}(K_v\tilde{\theta} + B_v\dot{\tilde{\theta}} - \tilde{\tau}_{ext}). \tag{18}$$

Based on the acceleration, the modified trajectories, θ_m, are calculated by integrating the modified acceleration.

In order to achieve effective pHRI with social robots, the robot's motion needs to be generated in accordance with the user's intent [14]. Moreover, in order to generate human-like motion, the motion range of human joints needs to be taken into account [4]. Additionally, generating active motions that align with the user's intention is essential for cooperative social interaction [25]. To address these requirements and enable effective pHRI, this paper proposes schemes for VAC. The methods for determining each admittance parameter are described in the subsequent section.

A. VARIABLE DAMPING

The damping parameter plays a significant role in determining the robot's dynamic characteristics. When the robot is moving slowly or coming to a stop, a high damping value allows for smooth motion with a slow velocity response to the external torque. Conversely, if the robot needs to move quickly or change direction promptly in response to the external torque exerted by the user, a lower damping value is required. To account for both cases, the damping parameter is adjusted based on the external torque as follows

$$B_v = \begin{cases} \alpha B_s, & \text{if} \quad |\hat{\tau}_{ext}| < \tau_{min} \\ \alpha(B_s - \triangle B), & \text{if} \quad \tau_{min} < |\hat{\tau}_{ext}| < \tau_{min} \\ \alpha B_f, & \text{if} \quad |\hat{\tau}_{ext}| > \tau_{max} \end{cases} \tag{19}$$

where

$$\triangle B = \frac{B_s - B_f}{|\tau_{max} - \tau_{min}|}(|\hat{\tau}_{ext}| - \tau_{min}),$$

α denotes the switching coefficient used to reflect the motion range of both humans and the robot; B_s and B_f represent the damping values for slow and fast velocity responses, respectively, based on the external torque applied; τ_{max} and τ_{min} denote the upper and lower boundaries of the external torque. Fig. 3 describes the proposed external torque based variable damping. When the operator intends to perform a fine movement or stop, the damping parameter is set to a high value since the applied torque by the operator is small, and the motion speed may be low. Conversely, if the operator wants to accelerate or change the robot's direction, the applied torque by the operator is increased, and the robot is accelerated as the damping value is reduced.

It is important for robots to generate human-like behavior in social interactions with humans [4]. Additionally, when generating trajectories, it is necessary to consider the robot's workspace to avoid any collisions or accidents that may occur if contact between joints occurs during motion. To address this problem, the damping is adjusted to reflect the range of motion of both humans and robots simultaneously. In order to

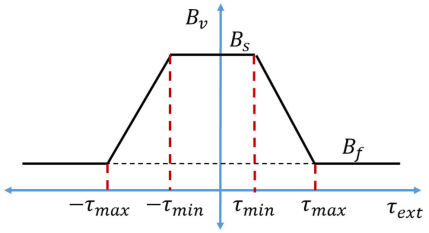

FIGURE 3. Variable damping according to an external torque.

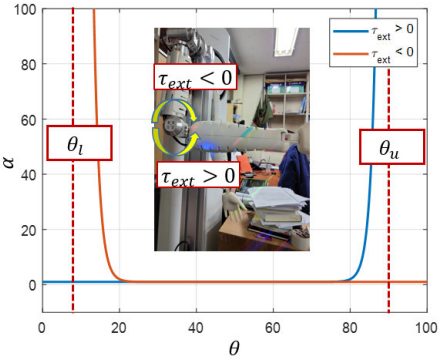

FIGURE 4. α according to the robot motion.

reflect the motion range, the damping coefficient α in eq. (19) is designed as follows:

$$\alpha = 1 + \beta^{\text{sign}(\hat{\tau}_{ext})(\theta - \bar{\theta})}, \tag{20}$$

where

$$\bar{\theta} = \begin{cases} \theta_u, & \text{if} \quad \hat{\tau}_{ext} > 0 \\ \theta_l, & \text{if} \quad \hat{\tau}_{ext} < 0 \end{cases}$$

β denotes a constant value that determines the changing rate of α according to joint angle; θ_u and θ_l denote the upper and lower boundaries of the motion range, respectively Fig. 4 shows that α varies according to the angle of the robot. In the available motion range, i.e., $\theta_l < \theta < \theta_u$, α is a small value, and the trajectory is generated according to the external force. On the other hand, when the trajectory of each joint of the robot deviates from the movable range of both humans and the robot, i.e., $\theta > \theta_u$ or $\theta < \theta_l$, α is dramatically increased. The damping is increased with α, and the trajectory is not modified by the external torque exerted by the user. By using this method, the damping is adjusted based on the user's intention while simultaneously taking into account the motion range of both humans and the robot during motion generation.

B. VARIABLE STIFFNESS

Typically, pHRI-based methods in industrial fields generate passive compliant motion of a robot according to a human's motion in cooperative tasks. However, in the case of a social robot, active motion for social interaction between participants, i.e., humans and the robot, is needed [25]. For active interaction, methods to generate the reference trajectory for handshaking and modify the trajectory with admittance control were proposed [14], [34]. However, to implement various

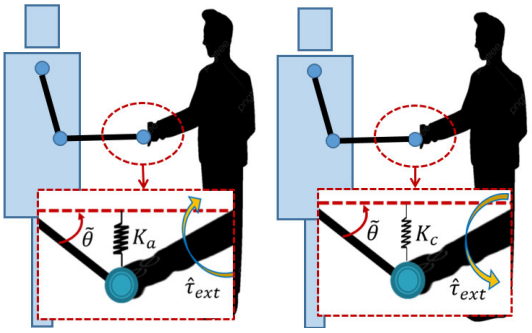

(a) Case of active motion. (b) Case of compliance motion.

FIGURE 5. Schematic of variable spring.

behaviors using these methods, predefined trajectories for each behavior are required.

To address the need for active motions in social robot interactions and enable various social gestures, this paper proposes a variable stiffness approach that classifies the user's intention based on the error between the reference and real angles, $\tilde{\theta}$, and the external torque exerted by the user. The variable stiffness is expressed as follows:

$$K_v = \begin{cases} K_a, & \text{if} \quad \text{sign}(\tilde{\theta} \cdot \hat{\tau}_{ext}) \geq 0 \\ K_c, & \text{if} \quad \text{sign}(\tilde{\theta} \cdot \hat{\tau}_{ext}) < 0 \end{cases} \tag{21}$$

where K_a and K_c respectively represent the joint stiffness for active and compliant motions of the robot. The active motion of the robot is generated based on the variable stiffness and $\tilde{\theta}$. When the direction of the active motion of the robot, i.e., the direction of $\tilde{\theta}$, aligns with the direction of the external torques, i.e., $\text{sign}(\tilde{\theta} \cdot \hat{\tau}_{ext}) \geq 0$ as shown in Fig. 5(a), it is assumed that the direction of the active motion of the robot is the same as the direction of the user's intended motion, and the active motion of the robot is generated based on the large stiffness, K_a, and $\tilde{\theta}$. Conversely, when the direction of $\tilde{\theta}$ is not aligned with the direction of the user's external torque, as shown in Fig. 5(b), the small stiffness K_c is employed, and the robot generates compliance motion in response to the external torque exerted by the user.

In this paper, the reference point is used to classify the user's intention and generate the active motion of the social robot. However, when the reference point is fixed, it becomes challenging to respond to various situations. If the reference point is not appropriate for the user's situation, such as their posture, body size, etc., it can lead to large external torques that disturb the user's motion. In order to address the problem, in this paper, a variable reference point is proposed:

$$\theta_d = \theta_0 + \gamma_t \int \hat{\tau}_{ext} dt, \tag{22}$$

where θ_0 and γ_t denote initial reference point and adjusting ratio according to τ_{ext}, respectively. When the reference point does not match the user's situation, the external torques exerted by the user increase, and the reference point is adapted based on the external torques. By using the adjusted

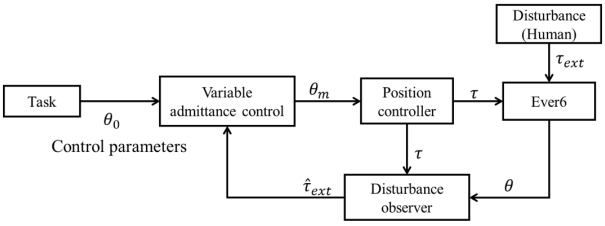

FIGURE 6. A block diagram for the proposed control loop.

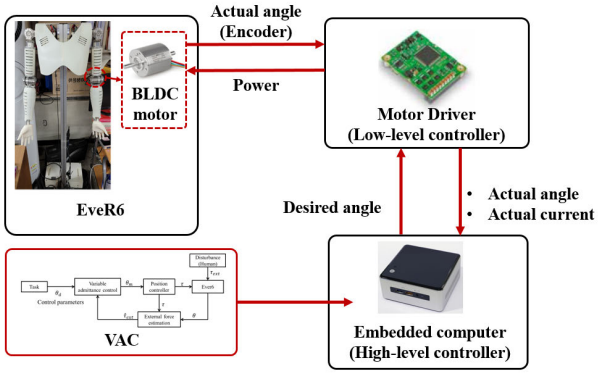

FIGURE 7. System diagram of EveR6.

reference point, active motion is generated to reflect various situations using the variable stiffness.

Fig. 6 shows the overall block diagram of the proposed methods. Control parameters of the proposed methods and the target angles of the robot, θ_0, are determined, and they are applied to proposed VAC schemes to generate the motions for the social gestures, θ_m. During the motion, if contact occurs between the human and robot, the external torques, denoted by $\hat{\tau}_{ext}$, are estimated using the disturbance observer based on the motor torque and actual angle of each joint, i.e., τ and θ. The estimated torques are then used to modify the trajectories based on the proposed schemes for pHRI. Finally, the robot follows the motion generated based on the position controller.

V. PERFORMANCE VALIDATION

A. SYSTEM CONFIGURATION

To demonstrate the effectiveness and evaluate the performance of the proposed methods, experiments were conducted using the dual-arm robot, EveR6, to realize the social gestures. The system configuration of the EveR6 is described in Fig. 7.

The proposed method is implemented on an embedded computer (Intel, NUC6i3SYK), with a control loop sampling time of 10 ms. Actual joint angles of the robot are measured by encoders (Maxon, Encoder 16 EASY) at each joint. The measured values of actual angles and currents are acquired from a BLDC driver (Maxon, EPOS4), and they are sent to the high-level controller, which is the embedded computer. In the high-level controller, trajectories are generated for each task, and the control commands to follow the trajectories are computed in the motor driver, which is the low-level controller, and sent to the commercial BLDC motors of each joint. Each joint of the robot is driven by the motors with a harmonic

TABLE 3. The motor specifications of the Ever6.

i	Nominal torque	Stall torque	RPM	Gear ratio
1	0.151 Nm	1.940 Nm	4100	100:1
2	0.151 Nm	1.940 Nm	4100	100:1
3	0.073 Nm	1.090 Nm	6310	100:1
4	0.073 Nm	1.090 Nm	6310	100:1
5	0.011 Nm	0.074 Nm	12700	100:1
6	0.011 Nm	0.074 Nm	12700	100:1

gear, and the specifications of each motor are summarized in Table 3. When contact occurs between the user and the robot during motion, the external torques are estimated using the GM-based disturbance observer with measured actual angles and currents. The proposed VAC schemes modify the trajectories based on the estimated external torques, and the robot follows the modified trajectories.

The parameters of the admittance control are determined based on the response of a second-order system. To determine the admittance parameters, it is assumed that the admittance coefficients remain constant under specific conditions, such as $|\hat{\tau}_{ext}| < \tau_{min}$ or $|\hat{\tau}_{ext}| > \tau_{min}$. The model of each joint in eq. (17) is expressed in the Laplace domain [15]:

$$\frac{\Theta(s)}{T(s)} = \frac{m}{s^2 + (b_v/m)s + (k_v/m)} \triangleq \frac{b_0}{s^2 + 2\zeta\omega_n^2 s + \omega_n^2}, \tag{23}$$

where ω_n and ζ denote natural frequency and damping ratio of the system, respectively. In this paper, the model of each joint was designed as a critically damped or overdamped system to prevent overshoot. The condition for determining the stiffness and mass of the model is obtained by

$$\zeta = \frac{b_v}{2\sqrt{mk_v}} \geq 1. \tag{24}$$

Taking the robot's specifications into account, the damping values, i.e. B_f and B_s, were determined approximately based on the speed of each joint relative to the torques, τ_{min} and τ_{max}. The mass was selected such that the settling time is less than 0.5 s. The stiffness for compliant motion, i.e. K_c, was designed to be 0, while the stiffness of each joint for active motion, K_a, was determined based on eq. (24). All the control parameters were finally fine-tuned through experimentation.

B. EVALUATION OF VARIABLE DAMPING ACCORDING TO MOTION RANGE

Before conducting experiments on social gestures, experiments were performed to investigate the effect of variable damping on the robot's workspace. For these experiments, the motion range of the fourth joint, i.e., θ_u and θ_l from eq. (19), were assumed to be $\theta_u = 100$ degrees and $\theta_l = 30$ degrees. External torque estimation and motion generation for the fourth joint were performed based on the proposed method. The control parameters for these experiments were determined as follows: $\beta = 3.5$, $M = 0.05$, $B_s = 2.0$, $B_f = 0.5$, and the stiffness for active motion were not applied.

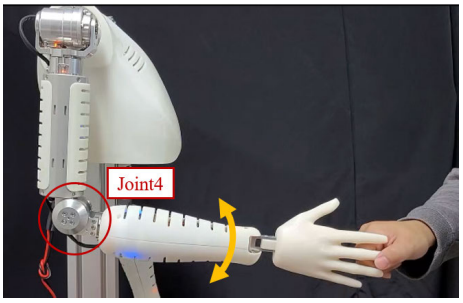

FIGURE 8. Experiment environment to show the effect of the switching coefficient.

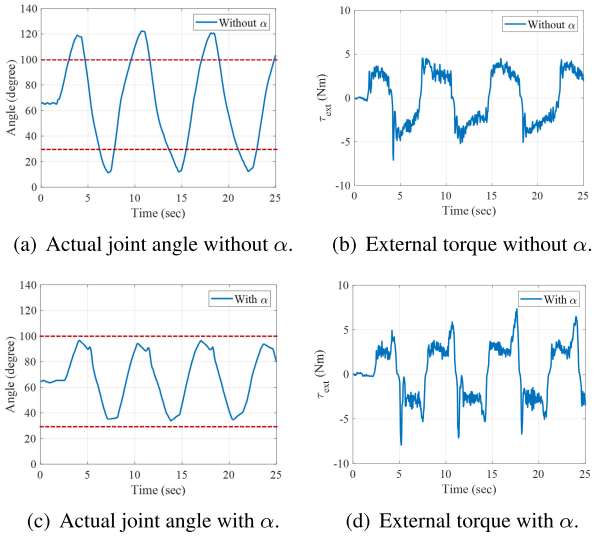

(a) Actual joint angle without α. (b) External torque without α.

(c) Actual joint angle with α. (d) External torque with α.

FIGURE 9. Result of the experiments about a variable damping to reflect workspace.

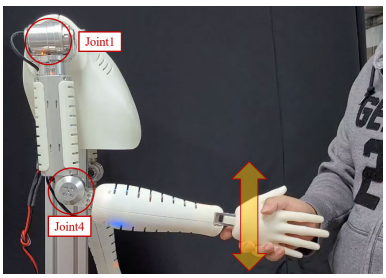

FIGURE 10. Experiment for handshaking.

In this experiment, the operator held the robot's arm and moved it up and down, as shown in Fig. 8. The experiment was conducted in two cases: with α and without α.

The results shown in Fig. 9 demonstrated the impact of applying α on the motion generation of the robot. When the α of eq. (19) was not applied, the motion according to the external torque was generated even at the upper and lower boundaries, as shown in Fig. 9(a). On the other hand, when the α was applied, the motion was not generated near the upper and lower boundaries, as shown in Fig. 9(b). From the results, it was confirmed that the proposed α reflects the workspaces of humans and the robot in motion generation.

TABLE 4. Control parameters for hand shaking.

Description	Joint1	Joint4
Initial reference angle (θ_0)	0 degrees	60 degrees
Mass (M)	0.050	0.005
Damping for slow response (B_s)	2	2
Damping for fast response (B_f)	1.0	0.5
Stiffness for active motion(K_a)	5.0	7.5
Stiffness for compliance motion (K_c)	0	0
Coefficient for variable reference angle (γ_t)	5	5

C. EXPERIMENT FOR THE SOCIAL GESTURE: HANDSHAKING

To demonstrate the effectiveness of proposed methods for pHRI in social interaction with humans, experiments to implement handshaking, one of the social gestures, were carried out. The scenario for the handshaking was designed as follows. Firstly, the robot moved to the initial pose for handshaking. Then, the user took the hand of the robot as shown in Fig. 10, and moved the hand up and down for handshaking. Through the motion of the human, external torques were generated, and the motion of the robot for the handshake was generated based on the proposed methods. Table 4 shows the initial angle of each joint and control parameters for the proposed VAC. The value of β used to calculate α was the same as in previous experiments. The external torques for the two joints of the robot that were mainly used for handshaking, i.e. the first and fourth joints, were estimated, and the pHRI motion for handshaking was generated based on the estimated torques.

Fig. 11(a) shows the estimated external torques. The user's motion results in external torques, and it was shown that the external torque exhibits a repetitive shape based on the user's motion. Based on the estimated torques, the motions for handshaking were generated with the proposed methods. Fig. 11(b) shows reference angles and modified trajectories based on proposed methods. The reference angles of the robot were modified according to the external torques, and applied to generate the motion for handshaking. The joint angles of the robot were modified based on the reference angles and the estimated torques, and the motion showed a repetitive pattern like handshaking.

Fig. 12 shows phase plots depicting the angular displacement and velocity of key joints. The figure confirms that the joint motions remained within a certain range and exhibited patterns that are similar to a circular one. From Fig. 11(b) and 12, it was demonstrated that the joint motions were effectively controlled, resulting in a stable handshake using the proposed method.

Additional experiments for handshaking were carried out in two cases to demonstrate the effectiveness of the variable reference angle: changing the pose during handshaking, as shown in Fig. 13, with a variable reference angle, and changing the pose of the human with a constant reference angle. The experiments were conducted using the same scenario as the previous experiment.

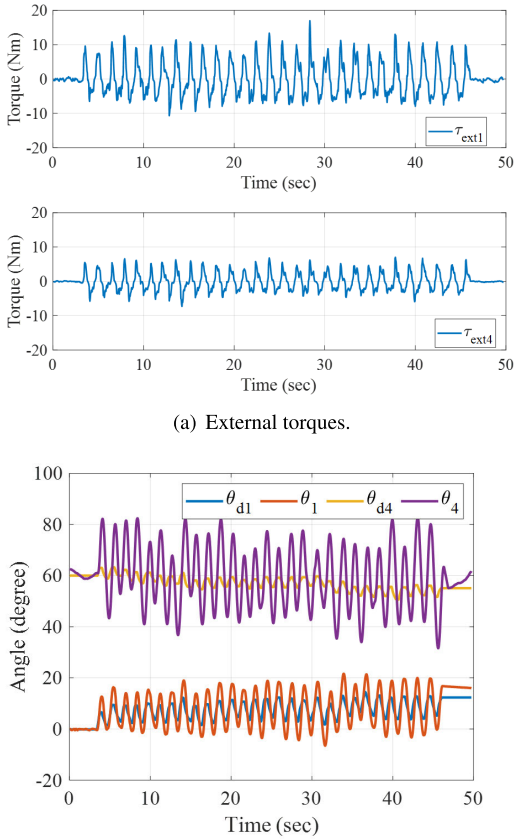

(a) External torques.

(b) Joint trajectories.

FIGURE 11. Experimental results in handshaking.

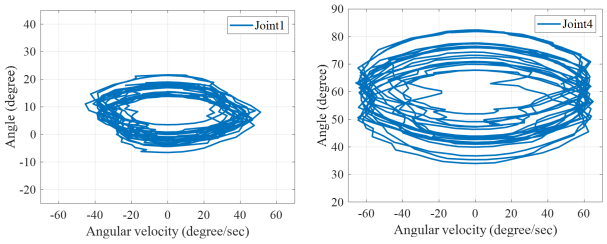

(a) Phase plot of the joint1.

(b) Phase plot of the joint4.

FIGURE 12. Phase plot of joint motions during handshaking.

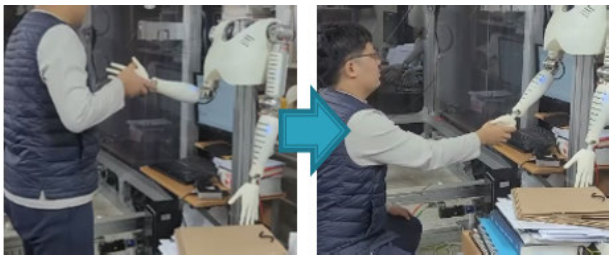

FIGURE 13. Experiment for handshaking with lowering his hand.

Fig. 14 shows the results of experiment with variable reference angles when the posture was changed. When the posture was changed, the external torques also changed according to the posture, and the variable reference angle was changed, as shown in Fig. 14(a). Based on the changed variable reference angles, the robot's angles were modified

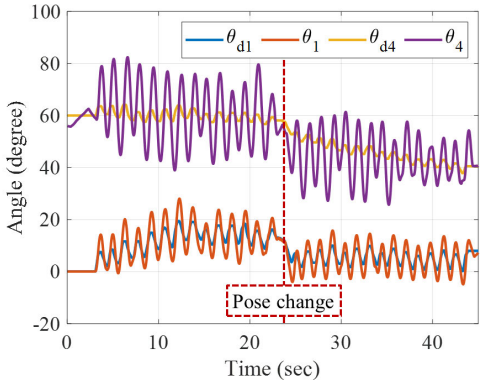

(a) Joint trajectories.

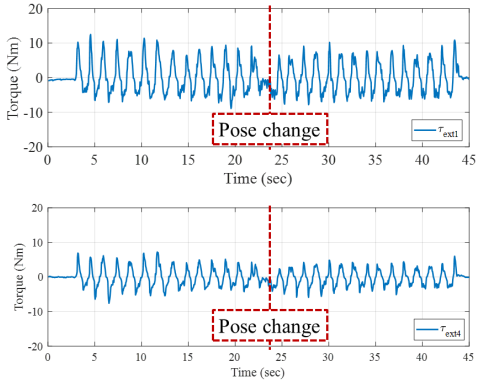

(b) External torques.

FIGURE 14. Experimental results in handshaking with a variable reference angle.

according to the changed pose: $\theta_1 = 7.83$ degrees and $\theta_4 = 40.69$ degrees.

Fig. 15 shows the results of experiment without variable reference when the pose was changed. The external torque changed according to the posture, but the reference angle was not changed. For this reason, the angles were modified in a similar range of the case without posture change as shown in Fig. 15(a). Since the reference angles of the robot were not adjusted to match the posture, the external torques were relatively larger than the case with the variable reference angle, as shown in Fig. 15(b). Comparing Fig. 14 with 15, it was demonstrated that the proposed methods can generate handshaking motions in various situations, even without predefined trajectories, by applying variable reference angles.

Fig. 16 shows phase plots depicting the angular displacement and velocity of key joints during handshaking with a pose change. In Fig. 16(a) and. 16(c), the joint motions before the pose change remained within a certain range, and after the pose change, the joint motions exhibited patterns that are similar to a circular one within a different specified range as shown in Fig. 16(b) and 16(d). From Fig. 14 and 16, it was shown that the joint motions were well controlled, and stable handshaking motions were generated based on the proposed methods.

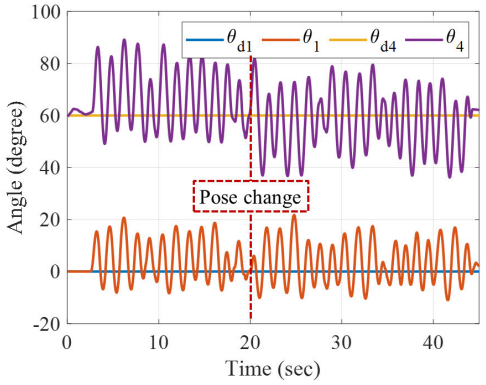

(a) Joint trajectories.

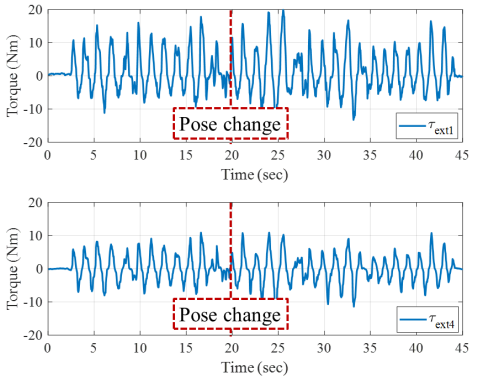

(b) External torques.

FIGURE 15. Experimental results in handshaking with a fixed reference angle.

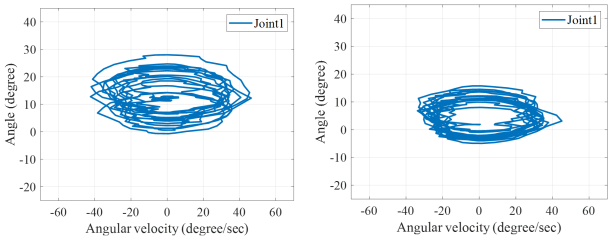

(a) Phase plot of the joint1 before changing the pose.

(b) Phase plot of the joint1 after changing the pose.

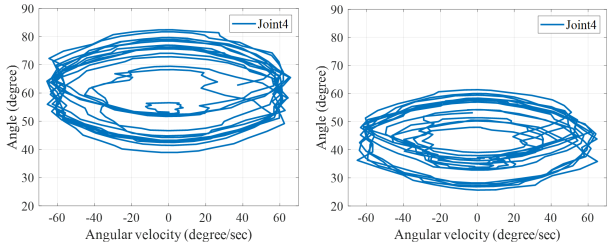

(c) Phase plot of the joint4 before changing the pose.

(d) Phase plot of the joint4 after changing the pose.

FIGURE 16. Phase plot of joint motions during handshaking with changing pose.

Based on the experimental results of handshaking, it has been confirmed that the proposed VAC-based methods successfully generate pHRI motions for the social gesture of handshaking by utilizing the user's external torques estimated with the sensorless disturbance observer.

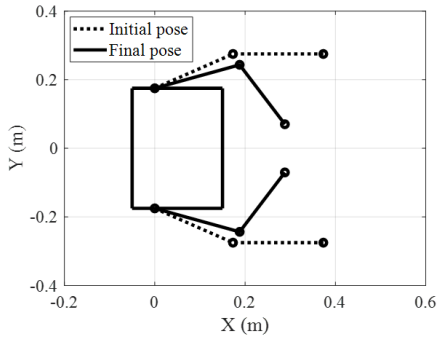

(a) Initial and final pose for hugging in Cartesian coordinate.

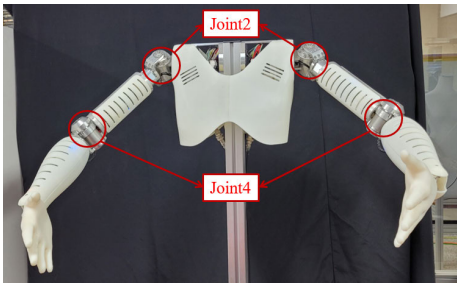

(b) Joints for hugging.

FIGURE 17. Experiment environment for hugging.

TABLE 5. Initial and final angles of the joints during hugging.

	Joint1	Joint2	Joint3	Joint4
Initial angle [degrees]	45	30	-50	30
Final angle [degrees]	45	20	-50	80

TABLE 6. Control parameters for hugging.

Description	Joint2	Joint4
Mass (M)	0.050	0.005
Damping for slow response (B_s)	2	2
Damping for fast response (B_f)	1.0	0.5
Stiffness for active motion(K_a)	5.0	7.5
Stiffness for compliance motion (K_c)	0	0
Coefficient for variable reference angle (γ_t)	5	10

D. EXPERIMENT FOR THE SOCIAL GESTURE: HUGGING

To demonstrate that the proposed schemes can generate various social gestures, beyond handshaking, experiments to implement hugging were conducted. The initial and final postures of the robot were determined to generate the hugging motion, as shown in Fig. 17(a), and the distance between the chest and arm of the robot at the final posture was 100 mm. The angles of each joint at the initial and final postures are summarized in Table 5. In this experiment, the second and fourth joints of each arm were primarily used to hug, as shown in Fig. 17(b). The external torques of the two joints were estimated, and the pHRI motion for hugging was generated based on the proposed methods. The control parameters for hugging are summarized in Table 6, and the value of β used to calculate α was the same as in previous experiments.

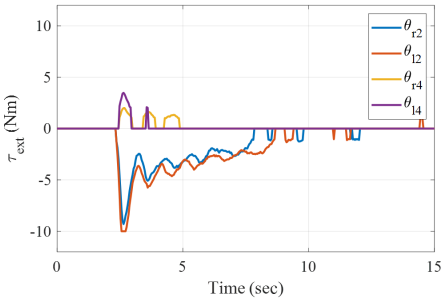

(a) External torques.

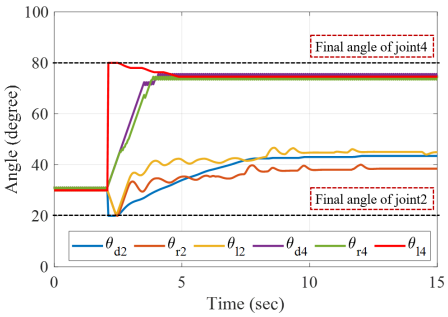

(b) Joint trajectories.

FIGURE 18. Experimental results in hugging the first target.

The robot moved from the initial posture to the final posture for hugging, and contact between the robot's arm and the human occurred when the person was positioned between the arm and chest of the robot. The external torques were caused by the contact between the human and the robot, and they were estimated by the sensorless disturbance observer. The estimated torques were applied to the proposed methods, and the motions for the social gesture of hugging were generated. To demonstrate that hugging with people of different body sizes is possible using the proposed method, experiments for hugging were conducted with two mannequins of different sizes. In the first case, the experiment of hugging was conducted with the first target, whose body width was about 500 mm, and in the second case, the experiment was conducted with the second target, whose body width was about 300 mm.

The results of the hugging experiment in the first case are shown in Fig. 18. External torques were caused by contact with the target, and they were estimated based on the disturbance observer as shown in Fig. 18(a). The estimated torques were used to generate the motion for the pHRI, and the interaction motions were generated as shown in Fig. 18(b). Based on the external torques, the reference angles of the second and fourth joints, i.e., θ_{d2} and θ_{d4}, were adjusted to 74.57 degrees and 43.49 degrees, respectively. The angles of the joints were modified based on the external torques and variable reference angles. The angles of the fourth joints of each arm were not modified much, while the angles of the second joints were modified by external torques to 38.49 degrees and 45.07 degrees.

The results of the hugging experiment with the second target were shown in Fig. 19. The external torques that

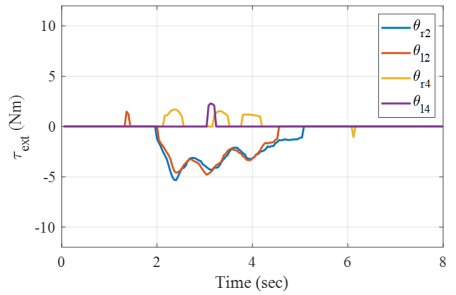

(a) External torques.

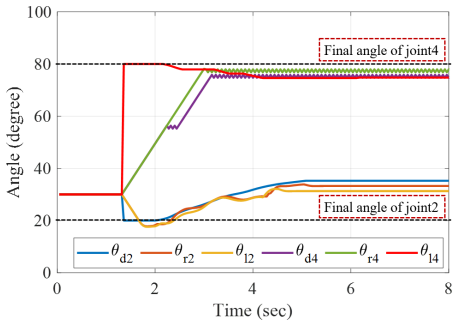

(b) Joint trajectories.

FIGURE 19. Experimental results in hugging the 2nd target.

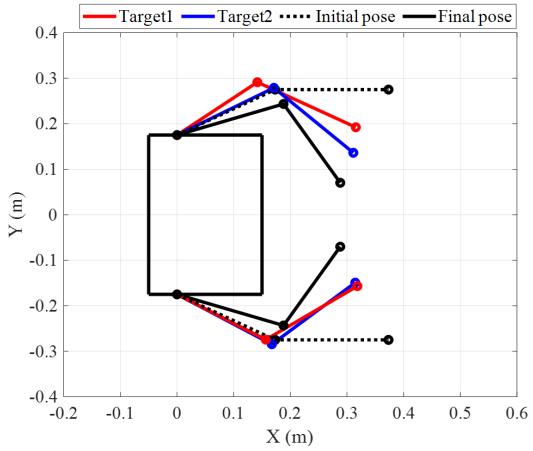

FIGURE 20. Comparison between experimental results according to the targets in Cartesian coordinate.

occurred during hugging were estimated based on the disturbance observer as shown in Fig. 19(a), and the pHRI motion for hugging was generated based on the estimated torques as shown in Fig. 19(b). Based on the external torques, the reference angles of the second and fourth joints, i.e., θ_{d2} and θ_{d4}, were adjusted to 74.78 degrees and 35.24 degrees, respectively. The angles of the joints were modified according to the external torques and variable reference angles to 33.24 degrees and 31.29 degrees, respectively, which was a less modified value than in the first case.

Fig. 20 shows the results of the experiments for hugging with two targets in Cartesian coordinate. When a target was present, the robot's motion was modified based on the proposed methods, and it was demonstrated that the angles were modified more when the target was larger. These results confirmed that the motions for hugging as well as handshaking can be realized based on the proposed methods. Moreover, Fig. 20 shows that the pHRI motions for hugging according to the various body sizes can be generated.

VI. CONCLUSION

In this paper, VAC based methods for pHRI were proposed, which were implemented with a dual-arm social robot called EveR6. To realize the proposed methods for pHRI without additional sensors, a GM-based disturbance observer was employed, and the external torque was estimated based on the disturbance observer. To generate the motion for pHRI based on the estimated torque, firstly, a variable damping according to the external torques and the motion of the robot was proposed to adjust the robot's movement speed while reflecting the movable range of a human and the robot simultaneously. Secondly, a variable stiffness according to the reference angle is proposed to generate active motions for cooperative pHRI. Additionally, a variable reference angle is proposed, which is adjusted to generate interaction motion according to different situations.

To verify the performance of the proposed methods, experiments were conducted. Using the GM-based disturbance observer, the external torques exerted by the user were estimated in these experiments, and it was confirmed that the pHRI motions for the social robot were generated based on the estimated torques and the proposed methods. Through experiments to show the effect of α, it was confirmed that the movable ranges of humans and the robot were simultaneously reflected in motion generation. Moreover, experiments for handshaking and hugging demonstrated that pHRI motions for the social gestures were generated according to the user's intention based on the proposed variable damping and spring parameters. Additionally, it was shown that pHRI motions in various situations, such as changing pose and size of the target, were generated based on the proposed variable reference angle without predefined trajectories for each situation.

In the near future, additional studies will be carried out to evaluate how the generated social gesture are human-like through experiments with various people.

REFERENCES

[1] M. Dotoli, A. Fay, M. Miśkowicz, and C. Seatzu, "An overview of current technologies and emerging trends in factory automation," *Int. J. Prod. Res.*, vol. 57, nos. 15–16, pp. 5047–5067, Aug. 2019.

[2] T. Zhang, B. Zhu, L. Lee, and D. Kaber, "Service robot anthropomorphism and interface design for emotion in human–robot interaction," in *Proc. IEEE Int. Conf. Autom. Sci. Eng.*, Washington, DC, USA, Aug. 2008, pp. 674–679.

[3] M. J. Pinto-Bernal, N. Cespedes, P. Castro, M. Munera, and C. A. Cifuentes, "Physical human–robot interaction influence in ASD therapy through an affordable soft social robot," *J. Intell. Robot. Syst.*, vol. 105, no. 3, p. 67, Jul. 2022.

[4] V. Prasad, R. Stock-Homburg, and J. Peters, "Human–robot handshaking: A review," *Int. J. Social Robot.*, vol. 14, no. 1, pp. 277–293, Jan. 2022.

[5] B. Siciliano and O. Khatib, *Springer Handbook of Robotics*. Berlin, Germany: Springer, 2016, pp. 1349–1360.

[6] J.-J. Cabibihan, A. El-Noamany, A. M. Ragab, and M. H. Ang Jr., "Guidelines for robot-to-human handshake from the movement nuances in human-to-human handshake," *Frontiers Robot. AI*, vol. 9, Mar. 2022, Art. no. 758519.

[7] Z. Wang, J. Yuan, and M. Buss, "Modelling of human haptic skill: A framework and preliminary results," in *Proc. World Congr. Int. Fed. Autom. Control*, Seoul, South Korea, Jul. 2008, pp. 14761–14766.

[8] M. Okuda, Y. Takahashi, and S. Tsuichihara, "Human response to humanoid robot that responds to social touch," *Frontiers Robot. AI*, vol. 12, no. 18, p. 9193, 2022.

[9] A. E. Block, S. Christen, R. Gassert, O. Hilliges, and K. J. Kuchenbecker, "The six hug commandments: Design and evaluation of a human-sized hugging robot with visual and haptic perception," in *Proc. 16th ACM/IEEE Int. Conf. Hum.-Robot Interact. (HRI)*, Boulder, CO, USA, Mar. 2021, pp. 380–388.

[10] K. Dautenhahn, "Socially intelligent robots: Dimensions of human–robot interaction," *Phil. Trans. Roy. Soc. B, Biol. Sci.*, vol. 362, no. 1480, pp. 679–704, Apr. 2007.

[11] M. Jindai, S. Ota, and T. Sasaki, "A hug behavior generation model based on analyses of human behaviors for hug robot system," in *Proc. Int. Conf. Design, Mech. Mater. Eng.*, Auckland, New Zealand, Sep. 2016, Art. no. 01011.

[12] V. Prasad, R. Stock-Homburg, and J. Peters, "Learning human-like hand reaching for human–robot handshaking," in *Proc. IEEE Int. Conf. Robot. Autom. (ICRA)*, Xi'an, China, May/Jun. 2021, pp. 3612–3618.

[13] A. Melnyk and P. Henaff, "Bio-inspired plastic controller for a robot arm to shake hand with human," in *Proc. Int. Conf. Design, Mech. Mater. Eng.*, Kyiv, UKraine, Apr. 2016, pp. 163–168.

[14] Z. Wang, A. Peer, and M. Buss, "An HMM approach to realistic haptic human–robot interaction," in *Proc. 3rd Joint EuroHaptics Conf. Symp. Haptic Interfaces Virtual Environ. Teleoperator Syst. (World Haptics)*, Salt Lake City, UT, USA, Mar. 2009, pp. 374–379.

[15] S. H. Kang, M. Jin, and P. H. Chang, "A solution to the accuracy/robustness dilemma in impedance control," *IEEE/ASME Trans. Mechatronics*, vol. 14, no. 3, pp. 282–294, Jun. 2009.

[16] Y. Maeda, T. Hara, and T. Arai, "Human–robot cooperative manipulation with motion estimation," in *Proc. IEEE/RSJ Int. Conf. Intell. Robots Syst.*, Maui, HI, USA, Oct./Nov. 2001, pp. 2240–2245.

[17] M. Rahman, R. Ikeura, and K. Mizutani, "Investigating the impedance characteristic of human arm for development of robots to co-operate with human operators," in *Proc. IEEE Int. Conf. Syst., Man, Cybern.*, Tokyo, Japan, Oct. 1999, pp. 676–681.

[18] Y. Li and S. S. Ge, "Human–robot collaboration based on motion intention estimation," *IEEE/ASME Trans. Mechatronics*, vol. 19, no. 3, pp. 1007–1014, Jun. 2014.

[19] V. Duchaine and C. M. Gosselin, "Investigation of human–robot interaction stability using Lyapunov theory," in *Proc. IEEE Int. Conf. Robot. Autom.*, Pasadena, CA, USA, May 2008, pp. 2189–2194.

[20] G. Kang, H. S. Oh, J. K. Seo, U. Kim, and H. R. Choi, "Variable admittance control of robot manipulators based on human intention," *IEEE/ASME Trans. Mechatronics*, vol. 24, no. 3, pp. 1023–1032, Jun. 2019.

[21] J. Buchli, F. Stulp, E. A. Theodorou, and S. Schaal, "Learning variable impedance control," *Int. J. Robot. Res.*, vol. 30, pp. 820–833, Apr. 2011.

[22] K. Kronander and A. Billard, "A online learning of varying stiffness through physical human–robot interaction," in *Proc. IEEE/RSJ Int. Conf. Intell. Robots Syst.*, Saint Paul, MN, USA, May 2012, pp. 1842–1849.

[23] P. Kormushev, S. Calinon, and D. G. Caldwell, "Robot motor skill coordination with EM-based reinforcement learning," in *Proc. IEEE/RSJ Int. Conf. Intell. Robots Syst.*, Taipei, Taiwan, Oct. 2010, pp. 3232–3237.

[24] J. Duan, Y. Gan, M. Chen, and X. Dai, "Adaptive variable impedance control for dynamic contact force tracking in uncertain environment," *Robot. Auton. Syst.*, vol. 102, pp. 54–65, Apr. 2018.

[25] K. Dai, Y. Liu, M. Okui, Y. Yamada, and T. Nakamura, "Variable viscoelasticity handshake manipulator for physical human–robot interaction using artificial muscle and MR brake," *Smart Mater. Struct.*, vol. 28, no. 6, Jun. 2019, Art. no. 064002.

[26] X. Zhang, J. Zhao, M. Zhang, and X. Liu, "Disturbance recognition and collision detection of manipulator based on momentum observer," *Sensors*, vol. 20, no. 15, p. 4187, Jul. 2020.

[27] C. Yang, G. Peng, L. Cheng, J. Na, and Z. Li, "Force sensorless admittance control for teleoperation of uncertain robot manipulator using neural networks," *IEEE Trans. Syst., Man, Cybern., Syst.*, vol. 51, no. 5, pp. 3282–3292, May 2021.

[28] A. Wahrburg, E. Morara, G. Cesari, B. Matthias, and H. Ding, "Cartesian contact force estimation for robotic manipulators using Kalman filters and the generalized momentum," in *Proc. IEEE Int. Conf. Autom. Sci. Eng. (CASE)*, Gothenburg, Sweden, Aug. 2015, pp. 1230–1235.

[29] S. Liu, L. Wang, and X. V. Wang, "Sensorless force estimation for industrial robots using disturbance observer and neural learning of friction approximation," *Robot. Comput.-Integr. Manuf.*, vol. 71, Oct. 2021, Art. no. 102168.

[30] J. Swevers, W. Verdonck, and J. D. Schutter, "Dynamic model identification for industrial robots," *IEEE Control Syst. Mag.*, vol. 27, no. 5, pp. 58–71, Oct. 2007.

[31] J. Jin and N. Gans, "Parameter identification for industrial robots with a fast and robust trajectory design approach," *Robot. Comput.-Integr. Manuf.*, vol. 31, pp. 21–29, Feb. 2015.

[32] T. Lee, B. D. Lee, and F. C. Park, "Optimal excitation trajectories for mechanical systems identification," *Automatica*, vol. 131, Sep. 2021, Art. no. 109773.

[33] D. Jung, H. Do, T. Choi, J. Park, and J. Cheong, "Robust parameter estimation of robot manipulators using torque separation technique," *IEEE Access*, vol. 9, pp. 150443–150458, 2021.

[34] Y. Wang, Y. Yang, B. Zhao, X. Qi, Y. Hu, B. Li, L. Sun, L. Zhang, and M. Q.-H. Meng, "Variable admittance control based on trajectory prediction of human hand motion for physical human–robot interaction," *Appl. Sci.*, vol. 11, no. 12, p. 5651, Jun. 2021.

JAEUK CHO received the B.S. degree in mechanical engineering from Konkuk University, South Korea, in 2011, and the M.S. degree in mechanical engineering from Hanyang University, in 2013, where he is currently pursuing the Ph.D. degree. His current research interests include robot dynamics and control, force control, humanoid robots, legged robots, social robots, and industrial robots.

DONGWOON CHOI received the B.S. and M.S. degrees in mechanical engineering from Hanyang University, South Korea, in 2005 and 2007, respectively, where he is currently pursuing the Ph.D. degree. He is a Senior Researcher with the Department of AI Robotics Research and Development, Korea Institute of Industrial Technology. His current research interests include robot dynamics and control, humanoid robots, android robots, social robots, and industrial robots.

JONG HYEON PARK (Member, IEEE) received the B.S. degree in mechanical engineering from Seoul National University, Seoul, South Korea, in 1981, and the M.S. and Ph.D. degrees from the Massachusetts Institute of Technology (MIT), Cambridge, MA, USA, in 1983 and 1991, respectively. Since 1992, he has been with the School of Mechanical Engineering, Hanyang University, Seoul, where he is currently a Professor. He was a Korea Science and Engineering Foundation Japan Society for the Promotion of Science Visiting Researcher with Waseda University, Tokyo, Japan, in 1999; a KOSEF-CNR Visiting Researcher with Scuola Superiore Sant'Anna, Pisa, Italy, in 2000; a Visiting Scholar with MIT, from 2002 to 2003; a Visiting Scholar with Purdue University, West Lafayette, IN, USA, from 2008 to 2010; and a Visiting Scholar with the University of Stuttgart, Germany, from 2019 to 2020. He was associated with Brooks Automation Inc., Chelmsford, MA, USA, from 1991 to 1992 and from 2001 to 2002. His current research interests include biped robots, robot dynamics and control, haptics, and biorobots. He is a member of the Korean Society of Mechanical Engineers, the Korean Society of Automotive Engineers, the Korean Society of Precision Engineering, and the Institute of Control, Robotics and Systems. For six years, he has served as a Senior Editor of the *Journal of Mechanical Science and Technology*.